The Thioredoxin-like Protein Rod-derived Cone Viability Factor (RdCVFL) Interacts with TAU and Inhibits Its Phosphorylation in the Retina*[S]

Ram Fridlich‡, Francois Delalande§, Céline Jaillard‡, Jun Lu¶, Laetitia Poidevin‖, Thérèse Cronin‡, Ludivine Perrocheau‡, Géraldine Millet-Puel‡, Marie-Laure Niepon‡, Olivier Poch‡‖, Arne Holmgren¶, Alain Van Dorsselaer§, Jose-Alain Sahel‡, and Thierry Léveillard‡

Rod-derived cone viability factor (RdCVF) is produced by the *Nxnl1* gene that codes for a second polypeptide, RdCVFL, by alternative splicing. Although the role of RdCVF in promoting cone survival has been described, the implication of RdCVFL, a putative thioredoxin enzyme, in the protection of photoreceptors is presently unknown. Using a proteomics approach we identified 90 proteins interacting with RdCVFL including the microtubule-binding protein TAU. We demonstrate that the level of phosphorylation of TAU is increased in the retina of the *Nxnl1*$^{-/-}$ mice as it is hyperphosphorylated in the brain of patients suffering from Alzheimer disease, presumably in some cases through oxidative stress. Using a cell-based assay, we show that RdCVFL inhibits TAU phosphorylation. *In vitro*, RdCVFL protects TAU from oxidative damage. Photooxidative stress is implicated in retinal degeneration, particularly in retinitis pigmentosa, where it is considered to be a contributor to secondary cone death. The functional interaction between RdCVFL and TAU described here is the first characterization of the RdCVFL signaling pathway involved in neuronal cell death mediated by oxidative stress. ***Molecular & Cellular Proteomics 8:1206–1218, 2009.***

Oxidative stress is suspected to play a major role in numerous age-related diseases (1) and neurodegenerative disorders (2). High levels of oxygen result in generation of reactive oxygen species that interact with proteins, lipids, or DNA and lead to cell dysfunction and death. In the eye, several diseases including glaucoma (3) and age-related macular degeneration (4) are associated with oxidative stress. Retinal degenerations are a prevalent cause of severe loss of vision. Retinitis pigmentosa is a monogenic disease in which mutations occur in genes that lead to the death of rod photoreceptors resulting in night blindness. After rods die, cone photoreceptors gradually die, resulting in blindness. Recent evidence has implicated oxidative damage as a contributor to death of cones in retinitis pigmentosa and to death of both photoreceptor cell types in age-related macular degeneration (5). After rods die, oxygen consumption in the outer retina is markedly reduced, and tissue oxygen levels become substantially elevated (6). This results in progressive oxidative damage to cones and gradual cone cell death, which can be slowed by antioxidants (7). The antioxidant defenses include vitamins, minerals, and the antioxidant enzymes glutathione, superoxide dismutase, hydrogen peroxidase, catalase, and thioredoxins (8). The protection of thioredoxin 1 (TRX1)[1] against retinal photooxidative damage (9) and its role in neurodegenerative diseases like Alzheimer disease are known (10, 11). TRX1, the substrate of thioredoxin reductase, can protect neuronal cells by scavenging free radicals, binding and inhibiting apoptosis signal-regulating kinase 1 (12), regulating transcription factors, and maintaining redox homeostasis (13). Rod-derived cone viability factor (RdCVF) belongs to the family of thioredoxins (14). RdCVF is a trophic factor secreted by rods that promotes cone viability encoded by the nucleoredoxin-like 1 (*Nxnl1*) gene, also called thioredoxin-like 6. The loss of rods results in a decrease of RdCVF expression, which presumably leads to cone death due to a lack of trophic support (15, 16). The TRX active site containing two cysteines (C*XX*C) catalyzes the reduction of disulfide bonds in targeted

From the ‡Institut de la Vision, INSERM UMR592, 17 rue Moreau, 75012 Paris, France, §Laboratoire de Spectrométrie de Masse Bio-Organique, Institut Pluridisciplinaire Hubert Curien-Département Sciences Analytiques et Interactions Ioniques et Biomoléculaires, Université Louis Pasteur, CNRS, UMR7178, 25 rue Becquerel, 67087 Strasbourg, France, ¶Department of Medical Biochemistry and Biophysics, Medical Nobel Institute for Biochemistry, Karolinska Institute, SE-17177 Stockholm, Sweden, and ‖Laboratoire de Bioinformatique et Génomique Intégratives, Institut de Génétique et de Biologie Moléculaire et Cellulaire, 67404 Illkirch, France

Received, August 29, 2008, and in revised form, March 3, 2009

Published, MCP Papers in Press, March 11, 2009, DOI 10.1074/mcp.M800406-MCP200

[1] The abbreviations used are: TRX, thioredoxin; AD, Alzheimer disease; CDS, coding DNA sequence; GSK-3β, glycogen synthase kinase-3; RdCVF, rod-derived cone viability factor; RdCVFL, rod-derived cone viability factor long isoform; Nxnl1, nucleoredoxin-like 1; STRING, Search Tool for the Retrieval of Interacting Genes/Proteins; GO, gene ontology; aa, amino acids; HEK, human embryonic kidney; API5, apoptosis inhibitor 5; PARP1, poly(ADP-ribose) polymerase 1; HA, hemagglutinin; IAF, 5-(iodoacetamido)fluorescein.

proteins (17). The *Nxnl1* gene encodes two products via alternative splicing that contain an active site: a full-length protein (RdCVFL) that might carry a thioredoxin activity (18, 19) and a C-terminally truncated protein (RdCVF) with trophic activity for cones but without any enzymatic activity. This latter form resembles the cytokine TRX80, a form of human TRX1 that has no thioredoxin activity (20). The trophic effect is carried specifically by the short isoform RdCVF (14). The thiol oxidoreductase activity of RdCVFL has to date only been observed in the arthropod *Carcinoscorpius* (18), and the participation of RdCVFL in the protection of photoreceptors is currently unknown. To clarify the role of RdCVFL in photoreceptor survival, we identified a specific functional interaction between RdCVFL and TAU using a proteomics approach.

TAU protein is a microtubule-associated protein that has a role in assembly and stabilization of microtubules (21). In the brains of patients with Alzheimer disease (AD) TAU was found to be hyperphosphorylated (22), leading to aggregation of the protein and to a decrease in TAU binding to microtubules (23) resulting in cell death. Phosphorylated TAU is also toxic to neuronal cells (24). The interaction between RdCVFL and TAU is the first description of the participation of RdCVFL in the protection of photoreceptors and of a novel redox signaling pathway involved in regulating neuronal cell death.

EXPERIMENTAL PROCEDURES

Animal Models and Retina Extraction—Care and handling of mice in these studies conformed to the rules set by the Association for Research on Vision and Ophthalmology Resolution. Chicken retinal extracts are described in Fintz *et al.* (25). The *Nxnl1*$^{-/-}$ mice were generated on a pure BALB/c background. Retinas were solubilized in Nonidet P-40 lysis buffer (25 mM Hepes, pH 7.8, 1 mM EDTA, 1 mM DTT, 0.05 M KCl, 1% Nonidet P-40, 1 mM PMSF, protease inhibitors) followed by sonication and centrifugation. The soluble fraction was subjected to further analysis. Unless otherwise specified, all chemicals were obtained from Sigma.

GST-RdCVFL Affinity Chromatography—RdCVFL was cloned into pGEX-2TK plasmid (GH Healthcare, catalogue number 27-4587-01), overexpressed, and purified as described previously (14). GST and GST-RdCVFL were bound to Sepharose 4B beads (GE Healthcare), which were washed and packed in a column. An amount of GST and GST-RdCVFL equivalent in molarity was used. The columns were equilibrated with 25 mM Hepes, pH 7.8, 1 mM EDTA, 1 mM DTT, 0.05 M KCl. Chick retinas (postnatal day 17) were lysed in Nonidet P-40 lysis buffer followed by Polytron disruption and centrifugation. The soluble fraction was diluted to a concentration of 0.5 mg/ml and loaded on the equilibrated columns at a flow of 50 μl/min. After washing, elution was carried out with a KCl gradient (25 mM Hepes, pH 7.8, 1 mM EDTA, 1 mM DTT, 0.05–0.5 M KCl). Four fractions were collected from each column, desalted with Centricon (Amicon), and loaded on a gel followed by silver staining (ProteosilverPlus, Sigma). Lanes (except lane C) were cut out and subjected to MS analysis.

In-gel Digestion—In-gel digestion was performed with an automated protein digestion system, MassPREP Station (Waters). The gel slices were washed three times in a mixture containing 25 mM NH_4HCO_3, CH_3CN (1:1, v/v). The cysteine residues were reduced by 50 μl of 10 mM DTT at 57 °C and alkylated by 50 μl of 55 mM iodoacetamide. After dehydration with acetonitrile, the proteins were cleaved in gel with 40 μl of 12.5 ng/μl modified porcine trypsin (Promega) in 25 mM NH_4HCO_3 at 37 °C for 4 h. The tryptic peptides were extracted with 60% acetonitrile in 5% formic acid followed by a second extraction with 100% (v/v) acetonitrile.

Mass Spectrometry Analysis—The peptides extracted from the gel were directly analyzed by nano-LC-MS/MS. Nano-LC-MS/MS was performed on an Agilent 1100 Series HPLC-Chip/MS system (Agilent Technologies) coupled to an Ultra High-Capacity Trap mass spectrometer system (Bruker Daltonics). The voltage applied to the capillary cap was optimized to −1850 V. For tandem MS experiments, the system was operated with automatic switching between MS and MS/MS modes. The three most abundant peptides, preferring doubly charged ions, were selected on each MS spectrum for further isolation and fragmentation. The MS/MS scanning was performed in the ultrascan resolution mode at a scan rate of 26,000 *m/z* per second. A total of six scans were averaged to obtain a MS/MS spectrum. The complete system was fully controlled by ChemStation (Agilent Technologies) and EsquireControl (Bruker Daltonics) software. The mass data recorded during nano-LC-MS/MS analyses were processed and converted into .mgf peak list format.

Protein Identification—The MS and the MS/MS data were searched using a local Mascot server (version, Mascot 2.2.0; Matrix Science). The MS/MS data were analyzed against a composite target-decoy database including the National Center for Biotechnology Information (NCBI) protein sequences of human, *Rattus norvegicus*, *Mus musculus*, and Aves downloaded in February 2008 and reversed versions of these sequences (total 1,693,251 entries; see supplemental methods). Searches were performed with a mass tolerance of 250 ppm for MS mode and 0.4 Da in MS/MS mode for nano-LC-MS/MS analysis. One missed cleavage per peptide was allowed, and variable modifications were taken into account such as carbamidomethylation of cysteine, oxidation of methionine, and *N*-acetyl protein. Searches were performed without constraining protein molecular weight or isoelectric point and without any taxonomic restriction. To minimize false positive identifications, the results were subjected to very stringent filtering criteria. For the identification of a protein with two peptides or more, at least two unique peptides had to have a Mascot ion score above 25. In the case of single peptide hits, the score of the unique peptide must be greater (minimal "difference score" of 12) than the 95% significance Mascot threshold. The spectra of these single peptide hits are provided (supplemental data). For the estimation of the false positive rate, a target-decoy database search was performed (26, 27). In this approach peptides are matched against a database consisting of the native protein sequences found in the database (target) and of the sequence-reversed entries (decoy). The evaluations were performed using the peptide validation software Scaffold (Proteome Software). This strategy was used to obtain a final catalogue of proteins with an estimated false positive rate below 1%.

Bioinformatics—Protein-protein interactions were obtained from the STRING database (28) containing known and predicted physical and functional protein-protein interactions. STRING in protein mode was used, and only interactions with high confidence levels (>0.7) were kept. Network visualization was done with the Cytoscape software (29). We used the DAVID (Database for Annotation, Visualization and Integrated Discovery) functional annotation tool (30) to identify the enriched gene ontology (GO) terms within the gene lists. We used *p* values after Benjamini correction and considered only those where the corrected *p* value was inferior to 10^{-7}.

RNA Purification, Reverse Transcription-PCR, Plasmid Construction—Cone-enriched cultures were made as described previously (14, 25). Total RNA from chicken cone-enriched cultures was purified by cesium gradient (14) and subjected to RT analysis. PCR was performed with 100 ng of cDNA. Cycling conditions were as follow: 94 °C for 5 min followed by 35 cycles of amplification (94 °C dena-

turation for 30 s, annealing for 30 s at a temperature range of 52–58 °C, and 72 °C elongation for 1 min) with a final incubation at 72 °C for 3 min. Details of primers are provided in supplemental Table II. The PCR products of human *TRX1* and chicken *TAU* were cloned into the pCMV-HA/DEST vector (a gift from R. Roepman) by Gateway system cloning (BP and LR reactions). pCMV4-GSK-3β and the cDNA of human TAU (383 aa) were kindly provided by C. Gespach and I. Ginzburg, respectively. Chicken genomic DNA was purified using standard methods.

Cell Culture and Transfection—COS-1 and HEK 293 cells were grown in Dulbecco's modified Eagle's medium with 10% fetal bovine serum. The cells were transfected using the calcium phosphate coprecipitation technique (14). 48 h after transfection, cells were resuspended in lysis buffer (50 mM Tris, pH 7.5, 1 mM EDTA, 1 mM DTT, 50 μg/ml N^{α}-tosyl-L-lysinyl-chloromethyl ketone, 1% Triton X-100, protease inhibitors), sonicated, and centrifuged, and the supernatant was kept at −80 °C.

Co-immunoprecipitation—Diluted transfected cell extracts were incubated overnight with different antibodies. Immunocomplexes were immobilized on protein A-Sepharose beads. Beads were washed, and protein complexes were eluted by adding Laemmli buffer.

Western Blotting—Western blotting is described in Leveillard *et al.* (14). The antibodies used were as follows: anti-HA (Covance, catalogue number MMS-101R-0500; 1:1000), anti-RdCVF (RdCVF-N, 1:500), anti-Tau5 (Calbiochem, catalogue number 577801; 1:500), anti-AT8 (Autogen Bioclear, catalogue number 90206; 1:100), anti-actin (Chemicon, catalogue number MAB1501; 1:7500), and anti-human TRX1 (IMCO Corp., catalogue number ATRX-03; 1:1000).

Immunohistochemistry—*Nxnl1*$^{+/+}$ and *Nxnl1*$^{-/-}$ mice aged 10 months were used. Retinas were removed from eyes and fixed in 4% paraformaldehyde in 0.1 M phosphate buffer, pH 7.2, for 2 h. Immunohistochemistry was performed on 5-μm sections obtained from paraffin-embedded tissue blocks. TAU was visualized using anti-AT8 and -Tau5 antibodies. Sections were subjected to microwave irradiation for antigen retrieval. Nonspecific binding sites were blocked by incubation of sections for 1 h at room temperature with normal goat serum in PBS. Sections were incubated overnight at 4 °C with AT8 antibody (1:250) in PBS. Immunostaining was visualized using the avidin-biotin system (Vectastain, Vector Laboratories) and nitro blue tetrazolium/5-bromo-4-chloro-3-indolyl phosphate as the chromogen. After washing, sections were mounted in Vecstatin and imaged with a microscope (Leica).

In Vitro Thiol Oxidoreductase Assay—GST and GST-RdCVFL were eluted from beads using a buffer containing 10 mM glutathione. GST, GST-RdCVFL (in PBS), and the recombinant human TAU protein samples (Sigma, catalogue number T9392) in 50 mM MOPS, pH 6.8, 100 mM NaCl, 1 mM EDTA, 5 mM DTT, 1 mM PMSF were dialyzed against 50 mM Tris-HCl, pH 7.5, 1 mM EDTA overnight with Dispo-Biodialyzer devices (molecular mass cutoff, 10 kDa) (Sigma). 1 μM TAU protein was mixed with 2 μM GST or GST-RdCVFL. The mixture or TAU protein alone was treated with 200 μM H_2O_2 for 2 h at room temperature. The oxidized TAU was incubated with the thioredoxin system (500 μM NADPH (Sigma), 100 nM recombinant thioredoxin reductase, 20 μM thioredoxin1 (IMCO Corp., catalogue number TRX-01)) for 1 h. The free cysteines of the proteins were labeled by 100 μM fluorescent 5-(iodoacetamido)fluorescein for 20 min. This labeling was stopped by addition of 50 mM iodoacetamide. The sample loading buffer with or without 50 mM DTT was incubated with the samples at 56 °C for 20 min, and the proteins were separated on a gel. The fluorescent bands were detected under a UV light, and subsequently the protein bands were detected by Coomassie Blue staining.

On-line Supplemental Material—Supplemental Table I displays the 44 and 121 proteins that were identified as GST- and GST-RdCVFL-interacting proteins, respectively. Supplemental Table II displays the sequence primers used in this study. Supplemental data display the spectra of all the proteins identified with one peptide. Recombinant protein sequences used in the study are provided in supplemental Table III.

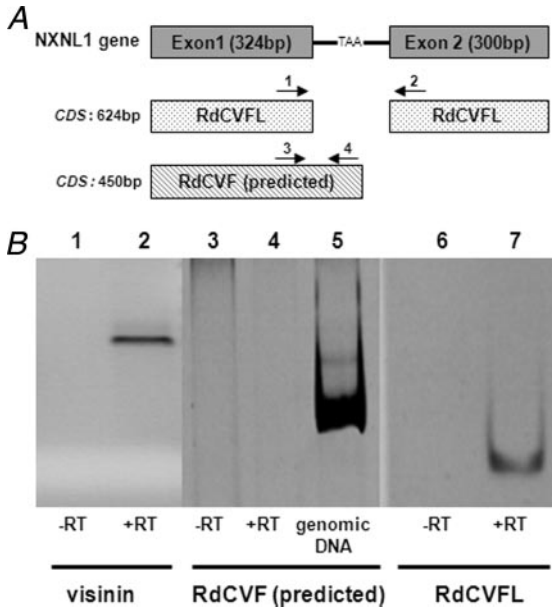

FIG. 1. **RdCVFL is expressed in chicken cone-enriched cultures.** *A*, schematic presentation of the chicken *Nxnl1* gene and its products. RdCVFL is composed of two exons (CDS, 624 bp), and RdCVF (predicted) is composed of the first exon and a part of the first intron (CDS, 450 bp). The *arrows* with *numbers* correspond to the primers used for RT-PCR. *B*, RT-PCR analysis on chicken cone cultures. Specific primers were used for the detection of RdCVF (predicted) (*lanes 3–5*) and RdCVFL (*lanes 6–7*). For controls visinin primers were used (*lanes 1–2*) as well as genomic DNA for primers 3 and 4 (*lane 5*).

RESULTS

RdCVFL Is Expressed in Cone-enriched Cultures—RdCVF was originally identified using cone-enriched cultures from chicken embryos. Bird retinas are cone-dominated, and in culture, cones represent 70% of the cell population (25). In the mouse retina RdCVF and RdCVFL are encoded by two alternative mRNA transcripts corresponding to exon 1 and to the spliced exons 1 and 2, respectively. In the chicken genome there is no in-frame stop codon immediately 3′ to exon 1 (31). We analyzed the expression of *NXNL1* mRNAs by RT-PCR in the cone-enriched culture (Fig. 1*A*). In these cultures, visinin is selectively expressed by cone cells (25). We detected an amplification product of RdCVFL mRNA but not RdCVF (Fig. 1*B*). The efficiency of RdCVF primers was validated on genomic DNA. The data demonstrate that RdCVFL is expressed by the chick cone culture.

Identification of RdCVFL-interacting Proteins—To identify RdCVFL-interacting proteins, we prepared soluble protein extract from chicken retina at postnatal day 17, a developmental stage rich in mature cones (result not shown). This retinal extract was loaded on GST-RdCVFL or GST columns. After washing, the elution was carried out with a 50–500 mM KCl

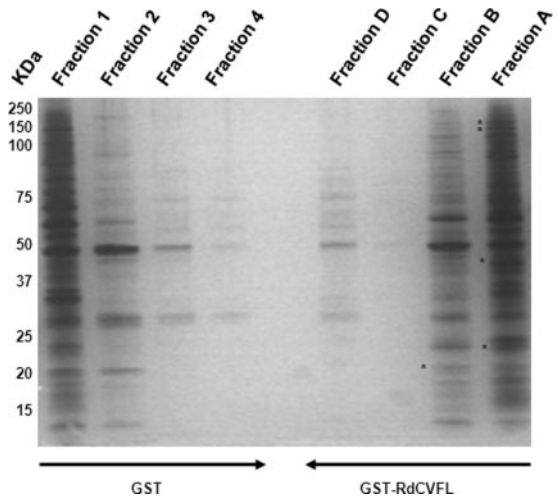

FIG. 2. **Silver-stained gel of GST- and GST-RdCVFL interacting proteins.** Soluble chicken retinal extracts were loaded on GST and GST-RdCVFL columns. Columns were washed, and four fractions were eluted from each column using a gradient of increasing KCl concentration. The first fractions (*1* and *A*) contain the lowest KCl concentration (50 mM), and the last fractions (*4* and *D*) contain the highest KCl concentration (500 mM). Proteins present in the GST-RdCVFL fractions and missing in the GST fractions are indicated by *asterisks* on the *left side* of the lane.

gradient. The eluted proteins collected in four fractions were loaded on a gel and silver-stained (Fig. 2). For both columns the amount of protein eluted decreased with increasing KCl concentration. Some differences in the eluted profile are indicated by an *asterisk* in Fig. 2. Each lane was cut into 2-mm slices corresponding to different molecular weights and subjected to proteomics analysis.

To identify the proteins, the trypsin-digested peptides in the individual slices were analyzed by nano-LC-MS/MS. Mass data collected during an LC-MS/MS analysis were processed and converted into a .pkl file to be submitted to the search software Mascot. A composite target-decoy database strategy was used to generate score criteria that yielded an estimated false positive rate of 1% (26). 44 and 121 proteins were identified as GST- and GST-RdCVFL-interacting proteins, respectively (supplemental Table I). After subtraction of the redundant proteins and the proteins eluted from the GST column, 90 proteins were found to interact specifically with RdCVFL (Table I). Among the proteins identified in this study, we found proteins related to apoptosis (apoptosis inhibitor 5 (API5) and poly(ADP-ribose) polymerase 1 (PARP1)) and linked to neurodegenerative diseases (TAU/MAPT (microtubule-associated protein Tau)). TAU was identified in several gel slices corresponding to molecular mass of 30–60 kDa by three different peptides (supplemental Table I).

RdCVFL Interactome—We analyzed the relation between the 90 identified proteins by bioinformatics. We searched in the STRING database for interactomic connections using the human orthologue of the chicken proteins. The STRING database contains predicted interactions that are based on several methods, including gene co-occurrence in genomes (*i.e.* phylogeny), gene co-expression, gene fusion events, genomic neighborhood (*i.e.* synteny), text mining, and experimental data such as co-immunoprecipitation and yeast two hybrid (28). To minimize the rate of false positives, we eliminated 43 of the 90 RdCVF partners using stringent criteria. Three major clusters were found: actin-interacting proteins and cytoskeleton proteins, ribosomal proteins, and proteins involved in translation and spliceosome proteins (Fig. 3). We noticed the presence of proteins of these three clusters eluted at highest salt concentration (fraction D in Table I). These 47 proteins represent the first comprehensive analysis of the RdCVFL network. To confirm our results, we tested for enrichment of gene ontology terms for the initial list of 90 proteins and the 49 negative control proteins (GST) (30). We observed a statistically significant enrichment of spliceosome proteins (GO RNA splicing, RNA binding, and ribonucleoprotein complex) (Table II). For the GST-interacting proteins all corrected p values were superior to 10^{-5}, representing only very weak enrichment (data not shown).

TAU, API5, and Ras-GTPase Are Expressed in Chicken Cone-enriched Cultures—The 90 proteins identified are expressed in chicken retina, but we focused on proteins co-expressed with RdCVFL in cones for their potential implication in neurodegenerative diseases. TAU is a microtubule-associated protein that has been identified in aberrant protein aggregates found in Alzheimer disease. API5 was initially isolated as a gene whose expression promoted cell survival following serum deprivation (32). The Ras-GTPase-activating protein SH3 domain-binding protein (G3BP) plays an important role in the trafficking of macromolecules between the cytoplasm and nucleus (33). Finally histone H2A is potentially involved in transcription regulation at the level of the chromatin.

We tested the mRNA expression of these RdCVFL-interacting proteins in the cone-enriched cultures. We detected the products of amplification of the mRNA encoding TAU, API5, and Ras-GTPase but not that of histone H2A (Fig. 4). This shows that TAU, API5, and Ras-GTPase are expressed in cones, whereas histone H2A, whose mRNA expression is cell cycle-dependent, is not present in cultured cone cells. We focused our analysis on the protein TAU because of its implication in neurodegenerative diseases and potentially in retinal degenerations.

Identification of Two Isoforms of TAU—In human brain, six TAU isoforms arising from alternative mRNA splicing of exons 2, 3, and 10 of the *TAU* gene have been identified (34). By RT-PCR, the primers referring to TAU detected several amplification products that form a smear in a range of 1000–1550 bp (Fig. 4). This is in agreement with the proteomics analysis (various molecular masses, range of 30–60 kDa) and may reflect the expression of several isoforms of TAU in the cones. To sequence the complete TAU coding DNA sequence (CDS), we amplified the chicken TAU products (detected as a

TABLE I

RdCVFL-interacting proteins identified by nano-LC-MS/MS

The first column lists the gene name for each protein. Four eluted fractions were collected. A, B, and D in the fifth column represent the KCl concentration at which the protein was eluted: A, 50–162.5 mM; B, 162.5–275 mM; and D, 387.5–500 mM. snRNP, small nuclear ribonucleoprotein; SH3, Src homology 3; Map, mitogen-activated protein; CNS, central nervous system; SNRPF, small nuclear ribonucleoprotein polypeptide F.

Symbol	Protein name	GI	kDa	Eluted fraction
ACTB	β-Actin	211055	9	D[a]
AMFR	Autocrine motility factor receptor	118096216	88	BD
API5	API5	57529974	59	AB
ATP6V1E1	Vacuolar H^+-ATPase E1	57525423	26	ABD
ATP6V1G1	ATPase, H^+-transporting	118099214	14	A
CAPZA1	F-actin-capping protein subunit α-1 (CapZ 36/32)	115592	33	B[a]
CAPZA2	F-actin-capping protein subunit α-2 (CapZ 36/32)	115579	33	D[a]
CAPZB	F-actin-capping protein subunit β isoforms 1 and 2 (CapZ 36/32)	115597	31	D[a]
CCT3	Chaperonin containing TCP1 (*Homo sapiens*)	119573352	61	D[a]
CPSF6	Cleavage and polyadenylation-specific factor 6	82233874	59	BD
DBN1	Drebrin	211726	72	D
DCAMKL1	KIAA0369	118084966	115	BD
DCD	Dermcidin (*H. sapiens*)	119617200	11	D
DDX3X	DEA(D/H) (Asp-Glu-Ala-(Asp/His)) box polypeptide 3	71895253	72	BD
DDX48	DEAD (Asp-Glu-Ala-Asp) box polypeptide 48	71897163	47	AD[a]
DDX5	DEAD (Asp-Glu-Ala-Asp) box polypeptide 5	45382259	67	BD
DDX6	DEAD (Asp-Glu-Ala-Asp) box polypeptide 6	118102030	54	B
DLAT	Dihydrolipoamide *S*-acetyltransferase	118102025	72	A[a]
DSTN	Destrin	53128989	19	D[a]
EEF1B2	Peptide elongation factor 1-β	4324407	25	D[a]
EEF1G	Eukaryotic translation elongation factor 1	118126430	6	A[a]
EFTUD2	U5 snRNP-specific protein	71895651	109	B[a]
EIF1AY	EIF1AY	71895237	16	A
EIF3S1	Eukaryotic translation initiation factor 3	61098232	29	AB[a]
EIF4A2	Translational eukaryotic initiation factor 4AII	21435808	46	AB[a]
ELAVL1	RNA-binding protein HuA	5738249	36	D[a]
ERH	Enhancer of rudimentary homologue	57529979	12	D
FKBP3	Putative FK506-binding protein	13992475	25	A
FUS	FUS/TLS	47420845	52	ABD[a]
FXR1	Fragile X mental retardation protein	50746068	64	B
G3BP	Ras-GTPase-activating protein SH3 domain-binding protein	57525015	52	B
GNAO1	Guanine nucleotide-binding protein	118096242	40	ABD
H1FX	Histone H1x	118096909	23	ABD[a]
HIST1H1E	Histone H1.01	121895	23	BD
HIST2H2AC	Histone H2A	71896919	14	ABD[a]
HIST2H2BE	Histone H2B	71895559	14	ABD[a]
HMGB3	HMG-1	391636	23	ABD
HNRPA0	Heterogeneous nuclear ribonucleoprotein A0	118097545	31	D[a]
HNRPH3	Heterogeneous nuclear ribonucleoprotein H3	60302824	17	D
HNRPK	Heterogeneous nuclear ribonucleoprotein K	50762370	47	ABD[a]
HNRPR	Heterogeneous nuclear ribonucleoprotein R	132626770	71	ABD[a]
HSD17B4	17-β-Hydroxysteroid dehydrogenase type IV	2315981	80	D
HSPA8	Heat shock cognate 70	2996407	71	AD[a]
HSPE1	Heat shock protein 10	2623879	11	A
KIAA1232	mKIAA1232	118089402	90	B
LASP1	LIM and SH3 protein 1 (*H. sapiens*)	119580947	30	D[a]
MAGOH2	MAGO protein	25990444	17	BD[a]
MAPK1	Chain A, structure of penta mutant human Erk2 Map kinase complexed with a specific inhibitor of human p38 Map kinase (*H. sapiens*)	157833528	43	A[a]
MAPT	CNS-specific microtubule-associated protein Tau	118102862	44	AB[a]
NPM1	Nucleophosmin 1 isoform 1	45383996	33	A[a]
NUDT16L1	Nudix	45382147	33	D
PAFAH1B1	Platelet-activating factor acetylhydrolase (PAF)	45383504	47	B
PARP1	PARP1	3220000	114	AB[a]
PKM2	Pyruvate kinase muscle isozyme	125608	58	AB[a]
PPP2R2A	α isoform of regulatory subunit B55, protein phosphatase 2	71894705	52	AD

TABLE I—*continued*

Symbol	Protein name	GI	kDa	Eluted fraction
PRDX1	Natural killer cell-enhancing factor	118094464	23	AD
PRP19	PRP19/PSO4 pre-mRNA processing factor 19 homolog (*H. sapiens*)	119594310	55	D
PRSS3	hCG22067 (*H. sapiens*)	119572363	30	ABD
RBBP4	Retinoblastoma-binding protein 4	45382339	48	B
RBMX	RNA binding motif protein, X-linked	119331082	41	D[a]
RPL23A	Rpl23a protein	118100216	18	D[a]
RPL30	Ribosomal protein L30	56118966	13	BD[a]
RPL5	RPL5	132989	34	D[a]
RPS10	Ribosomal protein S10	50760453	19	D[a]
RPS15A	Ribosomal protein S15	118098058	15	D[a]
RPS19	Ribosomal protein S19 (*M. musculus*)	12963511	16	BD[a]
RPS20	Ribosomal protein S20	118086993	17	A[a]
SDHA	Chain A, avian mitochondrial respiratory complex	110590574	68	ABD[a]
SDHB	Chain B, avian mitochondrial respiratory complex	110590575	29	D
SF3A1	Splicing factor 3a	71895509	88	B[a]
SFRS1	Splicing factor, arginine/serine-rich 1	166091440	28	D[a]
SMD1	Small nuclear riboprotein Sm-D	118086133	14	AD
SND1	Transcriptional coactivator p100	16660153	80	AB
SNRPA1	SNRPA1	50753184	28	ABD[a]
SNRPD3	Small nuclear ribonucleoprotein D3	56119060	14	BD[a]
SNRPF	SNRPF protein	118082523	10	B[a]
SNRPN	snRNP-B	10720263	25	ABD[a]
SPTBN1	Spectrin	118087525	274	AB
STAU	Staufen	61098218	78	BD
SUB1	Activated RNA polymerase II transcription cofactor 4	56605972	14	A
TAGLN3	Transgelin 3	50729726	22	A
THOC4	REF1-I	109492372	28	ABD[a]
TNC	Tenascin C	118099212	199	A
TNR	Tenascin R	45384054	148	AB
UQCRC2	Ubiquinol-cytochrome *c* reductase	118098350	49	D[a]
VIM	Vimentin	114326309	54	A[a]
WDR48	WD repeat domain 48	82231191	76	ABD[a]
XLRS1	X-linked juvenile retinoschisis protein (*M. musculus*)	5114035	26	ABD
YWHAG	YWHAG	71895543	28	B
ZNF207	ZNF207	118099726	53	A

[a] The proteins that figure in the interactome scheme (Fig. 3).

smear) and cloned the products into the pDEST/HA vector. We isolated two clones (Fig. 5*A*) and submitted the sequences of the isoforms 1 and 2 to NCBI under GenBank™ accession numbers EU380277 and EU380278 that correspond to the human isoforms 0N3R (352 aa) and 0N4R (383 aa), respectively. Both isoforms lack exons 2 and 3 present in the chicken TAU protein (GenBank accession number XM_424354). The N-terminal domain of isoform 1 is longer by 34 amino acids than the N-terminal of isoform 2, but the presence of an additional repeat domain (tubulin binding domain) in isomer 2 (exon 10) results in two proteins with similar length (Fig. 5*A*). We transfected COS-1 cells with plasmids encoding TAU isoforms 1 and 2 tagged with HA. By Western blotting analysis (anti-HA) we detected two bands of 68 and 66 kDa corresponding to isomers 1 and 2, respectively (Fig. 5*B*).

Mapping of the Interaction between RdCVFL and TAU—To validate the interaction between RdCVFL and TAU, we performed several co-transfections followed by co-immunoprecipitations followed by Western blot. First we transfected RdCVFL and isoform 1 of chicken TAU in COS-1 cells. The input lane shows that RdCVFL and TAU were expressed after transfection (Fig. 6*A*). When precipitated with anti-RdCVF-N antibodies (14) the Western blot using anti-HA (TAU was tagged with HA) revealed the presence of co-immunoprecipitated TAU protein (*lane 2*). Conversely precipitation of TAU with anti-HA led to the presence of RdCVFL in association with TAU (*lane 3*). We then assessed the specificity of this interaction by testing another member of the thioredoxin superfamily, TRX1. COS-1 cells were transfected with HA-TRX1 and HA-TAU (Fig. 6*B*). Because both proteins are tagged with HA, the immunoprecipitation with anti-HA revealed the presence of both proteins (*lane 3*). When precipitation was carried out with anti-TRX1, we only detected TRX1 and not TAU demonstrating the absence of an interaction between TRX1 and TAU (*lane 2*). We also tested RdCVF, the trophic factor (Fig. 6*C*). The immunoprecipitation of TAU did not co-precipitate RdCVF (*lane 3*). Altogether these results indicate that TAU interacts specifically with RdCVFL.

TAU is composed of two main domains, a projection domain in the N terminus and a microtubule binding domain in

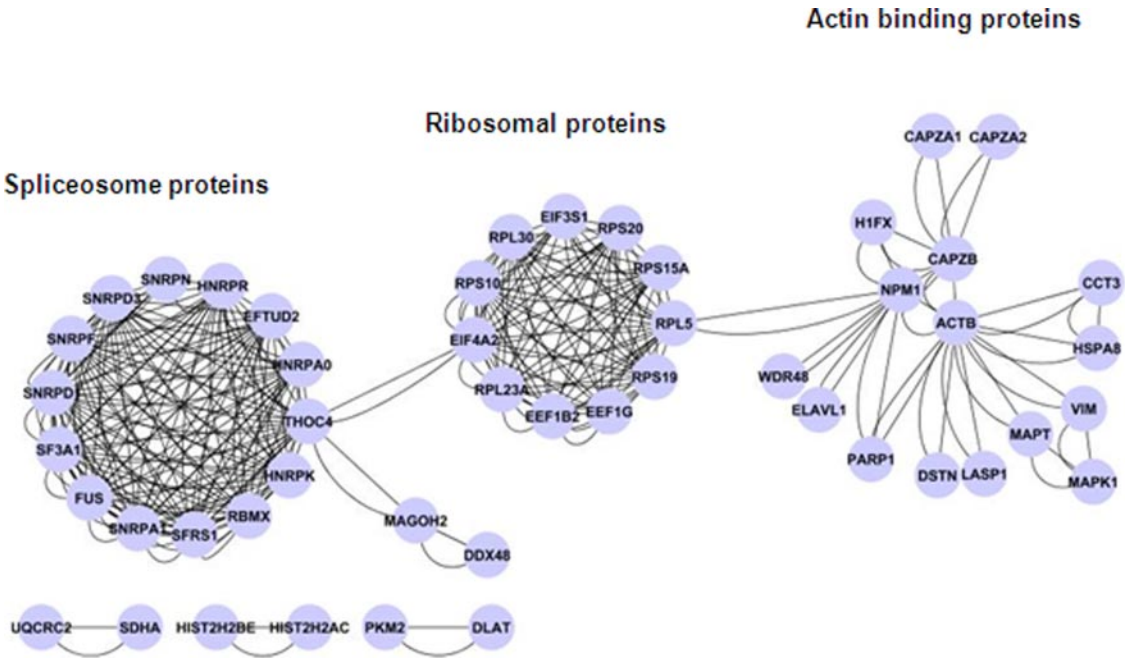

FIG. 3. **RdCVFL interactome network.** A graph of the RdCVFL network deduced from the identified RdCVFL-interacting proteins (Table I) is shown. Three clusters are displayed: actin-binding proteins, ribosomal proteins, and spliceosome proteins. The analysis of the proteins binding to GST, the negative control (supplemental Table I), as well as the high level of expression of their corresponding mRNA probed by Affymetrix gene chip indicate that the ribosomal proteins are more likely nonspecific binding proteins (data not shown).

TABLE II
Enrichment of gene ontology terms among RdCVFL-interacting proteins

Ontology categories and terms	No. of genes	*p* values
Biological process		
RNA splicing (GO:0008380)	17	2.6×10^{-10}
mRNA metabolic process (GO:0016071)	19	3.5×10^{-10}
mRNA processing (GO:0006397)	17	1.4×10^{-9}
RNA processing (GO:0006396)	18	5.4×10^{-7}
Molecular function		
RNA binding (GO:0003723)	31	2.1×10^{-15}
Protein binding (GO:0005515)	74	8.6×10^{-11}
Nucleic acid binding (GO:0003676)	47	7.9×10^{-7}
Cellular component		
Ribonucleoprotein complex (GO:0030529)	28	2.1×10^{-16}
Macromolecular complex (GO:0032991)	48	4.1×10^{-15}
Spliceosome (GO:0005681)	16	3.2×10^{-14}
Organelle part (GO:0044422)	52	2.5×10^{-13}
Intracellular organelle part (GO:0044446)	52	2.7×10^{-13}
Nuclear part (GO:0044428)	27	7.3×10^{-10}
Intracellular part (GO:0044424)	74	4.3×10^{-7}

the C terminus. Both domains bind to a subset of specific proteins. The sequences of 1–188 and 1–154 aa correspond to the projection domain in isomers 1 and 2, respectively, and the sequences 189–348 and 155–345 aa correspond to the microtubule binding domain in isomers 1 and 2, respectively. Fragments containing the projection domain and the microtubule binding domain were cloned into HA vector, and the interaction between the different domains and RdCVFL was tested by co-immunoprecipitation (Fig. 6*D*). RdCVFL was co-immunoprecipitated by anti-HA in the presence of co-transfected TAU microtubule binding domain (*lane 3*) but not TAU projection domain (*lane 6*; see also supplemental Fig. 1). These results show that RdCVFL interacts with the microtubule binding domain of TAU. Identical results were obtained using isoform 2 of TAU (results not shown).

TAU Is Hyperphosphorylated in the Retina of the Nxnl1$^{-/-}$ Mouse—The TAU protein was identified to be in a hyperphosphorylated form in protein aggregates in the brains of patients suffering from AD (22). It has been shown that oxidative stress caused by the inactivation of the gene coding for superoxide dismutase-2 or in a mitochondrial aldehyde dehydrogenase 2 dominant mutant increases the level of TAU phosphorylation (35, 36). Because RdCVFL has a potential thiol oxidoreductase activity, we analyzed the level of phosphorylated TAU in retina of *Nxnl1*$^{-/-}$ mice. *Nxnl1*$^{-/-}$ mice were created by homologous recombination of the entire exon 1 that encodes the short isoform RdCVF and the N-terminal part of RdCVFL on a BALB/c background.[2] RdCVFL was consequently absent in the retina of the *Nxnl1*$^{-/-}$ mouse as analyzed by Western blotting (Fig. 7*A*). Whereas the antibody Tau5 recognizes all forms of TAU independently of the phosphorylation state, AT8 recognizes TAU phosphorylated at residues Ser-202 and Thr-205. Retinas from *Nxnl1*$^{-/-}$ and *Nxnl1*$^{+/+}$ mice aged 11 days, 4 months, and 12 months were analyzed as well as brains

[2] T. Cronin, W. Raffelsberger, I. Lee-Rivera, M.-L. Niepon, B. Kinzel, E. Clerin, A. Petrosian, S. Picaud, O. Poch, J. A. Sahel, and T. Leveillard, manuscript submitted.

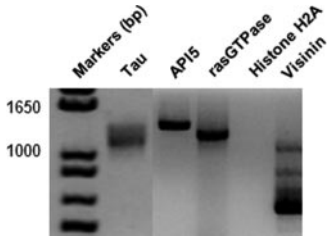

FIG. 4. ***TAU*, *API5*, and Ras-GTPase are expressed in cone-enriched culture from chicken embryos.** RT-PCR analysis was performed. Specific primers were used for the detection of *TAU*, *API5*, Ras-GTPase, and histone H2A. TAU cDNA was detected as a smear in the range of 1000–1550 bp. The visinin primers were used as a positive control. Amplification product lengths are as follows: *TAU*, 1266 bp; *API5*, 1572 bp; and Ras-GTPase, 1419 bp.

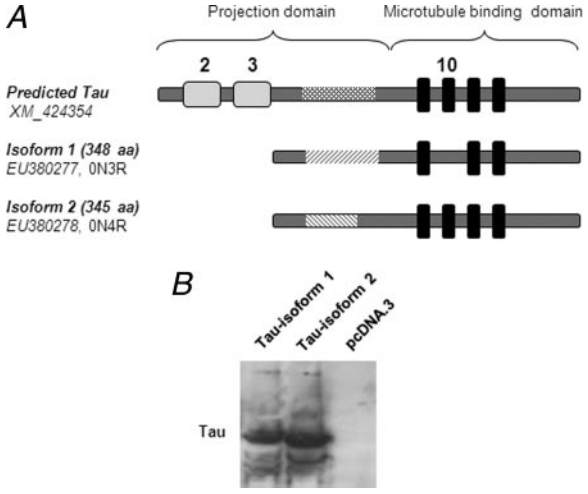

FIG. 5. **Identification of two novel isoforms of the TAU protein in the chicken retina.** *A*, schematic presentation of the predicted form and the two isoforms of chicken TAU. The predicted TAU, GenBank accession number XM_424354, contains in its N terminus exons 2 and 3 and in its C terminus exon 10. Isoforms 1 and 2 lack exons 2 and 3. Isoform 2 carries exon 10 resulting from alternative splicing. This supplementary exon in isoform 2 results in one more "tubulin binding domain" in the C terminus of the sequence. Between exons 3 and 10, the *shaded* regions differ between the two isoforms. *B*, transfection of isoforms 1 and 2 in COS-1 cells. The isoforms were tagged with the epitope HA, and Western blotting was carried out using anti-HA antibody. The two bands corresponding to the two isoforms, 68 and 66 kDa, respectively, were detected.

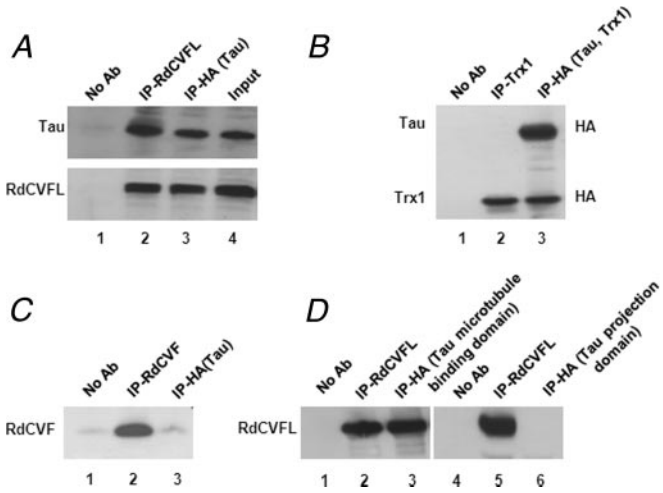

FIG. 6. **Mapping of the interaction between RdCVFL and TAU.** COS-1 transfections followed by co-immunoprecipitation and Western blotting were carried out to validate and to characterize the interaction between RdCVFL and TAU. As a negative control no antibody (*Ab*) was used for the immunoprecipitation (*IP*). *A*, co-immunoprecipitation of RdCVFL and chicken TAU tagged with HA. Anti-HA and anti-RdCVFL were used for the precipitation (*lanes 2* and *3*), and the Western blot of the immunoprecipitates was probed for HA and RdCVFL. *B*, co-immunoprecipitation of TRX1 and TAU. Both proteins were tagged with HA. Anti-HA antibody was used for immunoprecipitation (*lane 3*), and anti-TRX1 was used for the co-immunoprecipitation (*lane 2*). The Western blot of the immunoprecipitates was probed for HA. *C*, co-immunoprecipitation of RdCVF and TAU. Anti-RdCVF antibody was used for immunoprecipitation (*lane 2*), and anti-HA (*lane 3*) was used for the co-immunoprecipitation. The Western blot of the immunoprecipitates was probed for RdCVF. *D*, co-immunoprecipitations of RdCVFL and HA-TAU C-terminal (microtubule binding domain) and N-terminal (projection domain) fragments (*lanes 1–3* and *lanes 4–6*, respectively). Anti-RdCVF was used for immunoprecipitation (*lanes 2* and *5*), and anti-HA antibody was used for the co-immunoprecipitation (*lanes 3* and *6*). The Western blot of the immunoprecipitates was probed for RdCVFL.

from animals at 5 months. The analysis showed an increase in the expression of TAU (Tau5) at 5 and 12 months when compared with actin that is independent of the genotype. In the *Nxnl1*$^{-/-}$ retina TAU is hyperphosphorylated (AT8) compared with the aged-matched *Nxnl1*$^{+/+}$ retina (Fig. 7*A*). The increase in phosphorylation was also observed for the fetal isoform of TAU (labeled with an *asterisk*). No difference was detected in the level of TAU phosphorylation in the brain of the *Nxnl1*$^{-/-}$ mouse. This is consistent with the restricted expression of RdCVFL in the retina (14). We quantified the phosphorylated TAU (AT8) and normalized it to Tau5 and actin. There is a statistically significant increase in the excess of phosphorylation of TAU with age between 11 days and 5 and 12 months (Fig. 7*B*). To localize the hyperphosphorylated TAU, we performed immunohistochemistry with both TAU antibodies on retinal sections at 10 months. No difference was observed with Tau5 antibody, whereas the retina layers of the *Nxnl1*$^{-/-}$ mice had higher immunoreactivity for phosphorylated TAU (AT8; Fig. 7*C*). The inner nuclear layer, the outer nuclear layer, and to a limited extent the ganglion layer had a higher level of TAU phosphorylation consistent with the secretion of RdCVFL by rod photoreceptors.

RdCVFL Inhibits the Phosphorylation of TAU—Glycogen synthase kinase-3β (GSK-3β) is a kinase abundant in the brain and in the retina that phosphorylates TAU in transfection assays (37). Isoform 0N4R of human TAU (383 aa) corresponds to chicken isoform 1 (0N4R has no N-terminal inserts (N) and four microtubule binding repeats (R)). To examine the activity of RdCVFL on TAU phosphorylation by GSK-3β, we transfected HEK 293 cells with plasmids encoding RdCVFL, GSK-3β, and human TAU (Fig. 8*A*). Transfection of GSK-3β

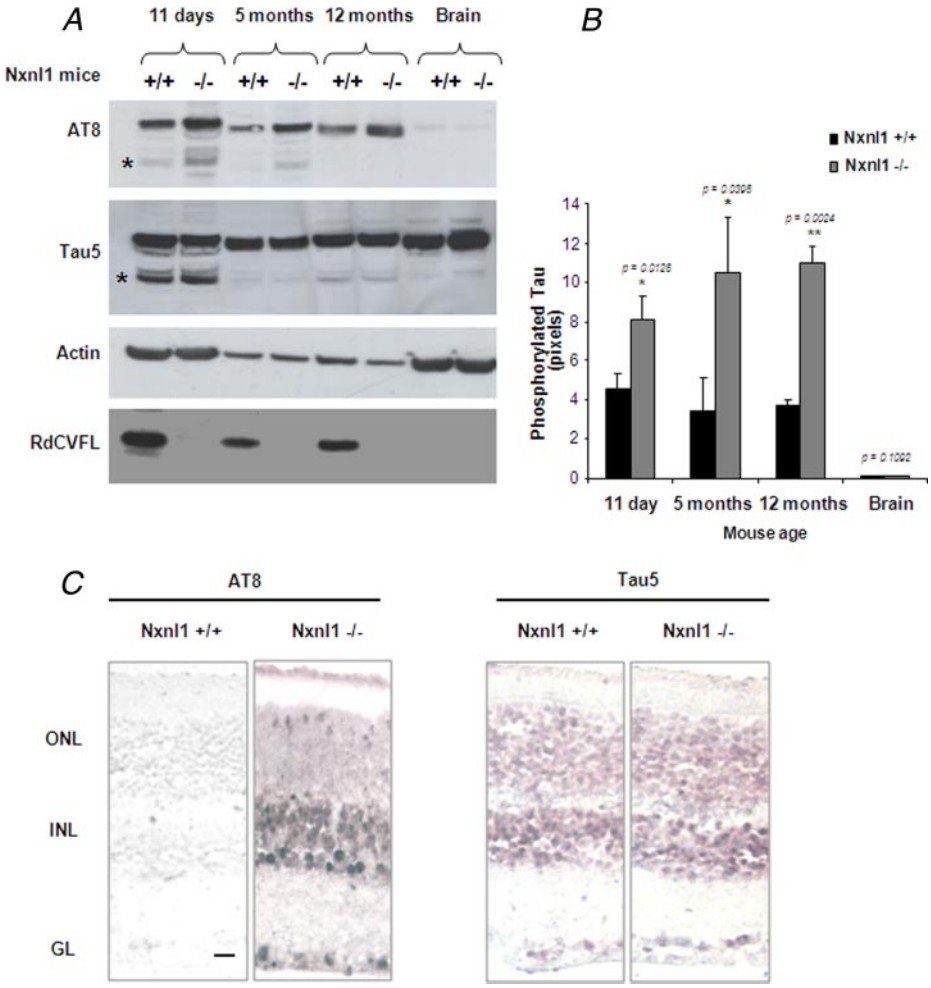

FIG. 7. **TAU is hyperphosphorylated in the retina of the *Nxnl1*$^{-/-}$ mouse.** *A*, the experiment was repeated on five different preparations. The results from a representative experiment are presented here. Retinas were dissected from 11-day-old, 5-month-old, and 12-month-old *Nxnl1*$^{+/+}$ and *Nxnl1*$^{-/-}$ (BALB/c background) mice and lysed in Nonidet P-40 lysis buffer. The extracts were analyzed by Western blotting using anti-AT8, anti-Tau5, anti-actin, and anti-RdCVFL antibodies. Extracts from brains of 5-month-old mice were also analyzed. The *asterisk* indicates the fetal form of TAU. *B*, quantitative analysis. The anti-AT8 bands were quantified using the lab-tool software. For normalization, we quantified the bands corresponding to AT8, Tau5, and actin. We divided the quantification value of AT8 by Tau5. The results were then divided by the value of actin. The ratio between *Nxnl1*$^{-/-}$/*Nxnl1*$^{+/+}$ at different ages is 1.75 (11 days), 3.00 (5 months), and 2.94 (12 months). Statistical analysis was preformed using a two-tailed paired *t* test. The *p* values are provided in the figure. *C*, distribution of phosphorylated TAU (AT8) and TAU (Tau5) in 10-month-old mouse retina. Immunostaining of *Nxnl1*$^{+/+}$ and *Nxnl1*$^{-/-}$ mice retina was carried out using AT8 and Tau5 antibodies. The two panels represents the same exposure time. *GC*, ganglion cells; *INL*, inner nuclear layer; *ONL*, outer nuclear layer. *Scale bar*, 10 μm.

led to an increase in phosphorylation of TAU as detected with AT8 antibody (*lanes 2* and *7*). The level of TAU phosphorylation was reduced by transfecting increasing amounts of RdCVFL (*lanes 7–10*). The expression of TAU and actin was only marginally affected. To demonstrate that the inhibition of TAU phosphorylation was a consequence of its specific interaction with RdCVFL, we repeated the experiment using TRX1, an enzymatically active thioredoxin that does not interact with TAU (Fig. 6*B*). Increasing the concentration of TRX1 did not reduce the level of phosphorylated TAU (*lanes 2–5*). The quantification of AT8 immunoreactivity normalized to Tau5 and actin demonstrated that RdCVFL inhibits TAU phosphorylation in a dose-dependent manner (Fig. 8*B*).

Protection of TAU Protein from Oxidation by RdCVFL—To evaluate the functional consequence of this interaction on the redox status of TAU *in vitro*, we studied the oxidation of TAU by H_2O_2 in the presence of RdCVFL. Free thiols in purified TAU were alkylated by fluorescent IAF (Fig. 9*A*). Incubation with H_2O_2 induced TAU oxidation and consequently the decrease in fluorescence (*lanes 4–5*). This decrease was of lower amplitude in the presence of GST-RdCVFL (*lane 6*). Oxidation of TAU led to a decrease of the 62-kDa protein band (TAU), which results from oxidative damage of the protein (Fig. 9*B*, *lanes 4–5*). Interestingly GST-RdCVFL protected the TAU protein from this damage, and the level of TAU was no longer changed by the H_2O_2 oxidation (*lane 6*). We next

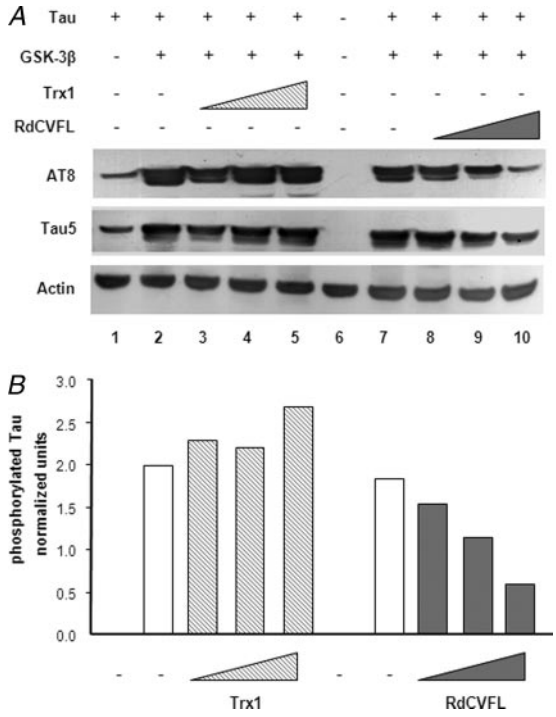

FIG. 8. **RdCVFL inhibits the phosphorylation of TAU.** The experiment was repeated five times independently and further verified in COS-1 cells. The results from a representative experiment are presented here. *A*, HEK 293 cells were transfected with a fixed amount of TAU and GSK-3β (700 and 450 ng, respectively) and increasing concentrations of RdCVFL (450, 900, and 1350 ng) (*lanes 8–10*). As a control, RdCVFL was replaced by TRX1 (used in the same range of concentrations as RdCVFL) (*lanes 3–5*). Cells were lysed, and the protein extraction was subjected to Western blotting against anti-AT8, anti-Tau5, and anti-actin. *B*, quantitative analysis. The AT8 bands were quantified using the lab-tool software. The values were normalized to total TAU (Tau5) and to actin (AT8/Tau5/actin). The *white columns* represent the level of phosphorylated TAU with GSK-3β addition in the absence of RdCVFL or TRX1.

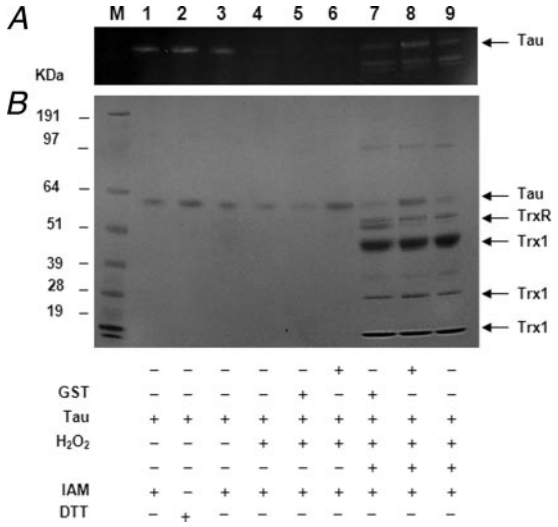

FIG. 9. **Protection of TAU protein from oxidation by RdCVFL *in vitro*.** Oxidation of TAU by H_2O_2 in the presence of RdCVFL (*lanes 1–6*) and in the presence of the thioredoxin system (*lanes 7–9*) is shown. *A*, free thiols in purified TAU were alkylated by fluorescent IAF. The reaction was subjected to different conditions as indicated (*lanes 1–9*). *B*, Coomassie Blue-stained gel of the reactions under the same conditions. The migration of the different proteins is indicated on the *right*. *IAM*, iodoacetamide. *Lane M*, molecular mass markers.

analyzed the subsequent reduction of TAU by the thioredoxin system (TRX1 + thioredoxin reductase), the main cellular protein disulfide reduction system (17). The thioredoxin system reduced the oxidized TAU protein, resulting in an increase of fluorescent IAF (Fig. 9*A*, *lane 9*) as reported previously (38). The level of fluorescence was even higher with GST-RdCVFL addition (Fig. 9*A*, *lane 8*), and the level of undamaged TAU protein (Fig. 9*B*, *lane 8*) was increased. These results show that the interaction of RdCVFL with TAU protects this protein from oxidative damage, and this protection assists in the reduction of TAU by the thioredoxin system.

DISCUSSION

RdCVF is a trophic factor belonging to the thioredoxin family. It is a spliced isoform of the *Nxnl1* gene that additionally encodes RdCVFL, a protein that contains a complete thioredoxin fold domain and most likely carries a thiol oxidoreductase activity. Nevertheless this enzymatic activity could only be demonstrated in its distant orthologue, the arthropod *Carcinoscorpius*, and not for the human protein (18, 19). The role of RdCVFL in photoreceptor survival was speculative. The functional interaction between RdCVFL and TAU described here demonstrates that in addition to the activity of RdCVF on cones the second isoform of the *Nxnl1* gene, RdCVFL, might participate in the protection of photoreceptors against oxidative stress.

To unravel the signaling pathway associated with RdCVFL, we used a proteomics approach to identify the RdCVFL-interacting proteins. The analysis of the RdCVFL interactome revealed three main clusters of proteins: ribosomal proteins, spliceosome proteins, and actin-binding proteins. Within the cluster of actin-binding proteins, the presence of microtubule-associated protein TAU, which is involved in neurodegenerative diseases, raises questions regarding the involvement of the TAU protein in photoreceptor degeneration.

TAU is a microtubule-associated protein that has a role in assembly and stabilization of microtubules. Twenty years ago, interest in the TAU protein arose when it was identified as a component of the paired helical filaments (39). Paired helical filaments contribute to neurofibrillary tangles and protein aggregates, the aberrant structures that were found in the brains of patients with AD; hence we focused our study on the interaction of RdCVFL with TAU. We demonstrated that RdCVFL as well as two newly described isoforms of TAU are expressed in the cone-enriched cultures and that RdCVFL interacts with TAU through the region containing a microtubule binding domain located at the C terminus of the protein. This region of the human TAU protein is enriched in phosphorylation sites that are grouped in two clusters located on both

sides of the microtubules binding domain with the exception of Ser-262/Ser-356 (located inside the binding domain itself) (23). TAU was demonstrated to exist in a hyperphosphorylated form in neurofibrillary tangles in the brains of patients suffering from AD (22) that leads to a decrease in the binding of TAU to microtubules and makes microtubules dynamically unstable (23). In addition, there is evidence that hyperphosphorylated TAU is associated with the induction of apoptotic cell death (24). This led us to assess the level of hyperphosphorylation of TAU in the retina of mice carrying a deletion of the *Nxnl1* gene. Both Western blotting and immunohistochemistry analyses demonstrated an increase in TAU phosphorylation in the neural retina in the absence of both products of the *Nxnl1* gene, RdCVF and RdCVFL. The fact that the TAU immunoreactivity was localized into the photoreceptor layer and to other inner retinal cells may be due to the secretion of RdCVFL as observed previously (14). The observation of an increase in phosphorylated TAU between 11 days (1.75-fold) and 5 months (3.00-fold) indicates that it is not related to any abnormality in the maturation of the retina but to a process involving environmental factors, most likely oxidative stress. The relation between hyperphosphorylation of TAU and RdCVFL was further demonstrated in a cell-based assay. The inhibition of TAU phosphorylation is specifically mediated by the interaction with RdCVFL and not by a general redox mechanism as shown by the lack of TRX1 activity in that assay. The mechanism of action of RdCVFL was addressed *in vitro*. RdCVFL was able to prevent the oxidative damage to the TAU protein induced by H_2O_2 and assisted in the reduction of TAU by the thioredoxin system. Our results demonstrate that RdCVFL plays a role in the inhibition of TAU phosphorylation and protects TAU against oxidative stress. One hypothesis is that RdCVFL, the protein with a thioredoxin catalytic site (CPQC), possesses an enzymatic activity toward its interacting substrate TAU. This activity controls the redox status of cysteine residues in the C-terminal domain of the TAU protein, and as reported previously, oxidized TAU is more accessible to phosphorylation than the reduced form (38, 40). The hyperphosphorylation of TAU promotes its aggregation (22), a consequence that may represent the first step toward the induction of neuronal cell death (Fig. 10). We propose that RdCVFL, which displays oxidoreductase-like features, is capable of chemically reducing TAU under oxidative stress conditions, stabilizing it and thereby inhibiting its phosphorylation. The role of RdCVFL in protecting retinal cells from apoptosis mediated by oxidative stress is supported by the fact that transfection of the cone-like cell line 661W with RdCVFL leads to cell protection against the death induced by photooxidative damage (19).

The contribution of this interaction to RdCVF signaling from rods to cones is still an open question. Because we showed that RdCVFL is expressed in the cone-enriched culture system, its position would be expected to be downstream of the activation of a putative RdCVF cell surface receptor. Alternatively and as reported earlier, *Nxnl1* is a bifunctional gene with the longer isoform RdCVFL participating in an intracellular mechanism of photoreceptor protection against oxidative stress. The participation of RdCVFL in cone rescue may be connected to its specific association with the spliceosome (Table II) that may reveal a role of RdCVFL in regulating the splicing. It is worth noting that the splicing protein U5-15K/DIM1 has a thioredoxin fold (41). Under oxidative stress condition this association may inhibit the splicing of the *Nxnl1* premessenger RNA and consequently enhance the production of the unspliced isoform RdCVF (42, 43). Oxidative stress has been implicated in the pathogeny of AD (44) and was shown at least in tauopathy models to proceed through the phosphorylation of TAU (45). Oxidative stress leads to the production of 4-hydroxynonenal and acrolein, which are found in the brain tissue of AD patients and favor TAU phosphorylation (46, 47). In animal models, the deficit in proteins controlling the production of free radicals such as superoxide dismutase-2 and aldehyde dehydrogenase 2 causes hyperphosphorylation of TAU (35, 36). All this combined evidence supports the role of oxidative stress in mediating TAU phosphorylation. The observation of abnormal TAU phosphorylation in a model lacking a thioredoxin family member strengthens the role of thioredoxin signaling in controlling the redox status of TAU and oxidative stress in neuronal tissues. Indeed this is the second time that an abnormal phosphorylation of TAU has been observed in the retina: hyperphosphorylated TAU was recently detected in the retina of patients suffering from glaucoma (48). The hyperphosphorylation of TAU in the retina of the *Nxnl1*$^{-/-}$ mouse (Fig. 7*C*) suggests that this mechanism is involved in triggering photoreceptor cell death in that model.[2] The description of the hyperphosphorylation of TAU in the retina, a tissue particularly vulnerable to photooxidative damage, may extend its role in neurodegeneration and the relevance of oxidative stress. Although RdCVF expression is restricted to the retina, its paralogue, RdCVF2, is also expressed in the brain (31). This opens the possibility that the RdCVF family members may be involved in regulating TAU

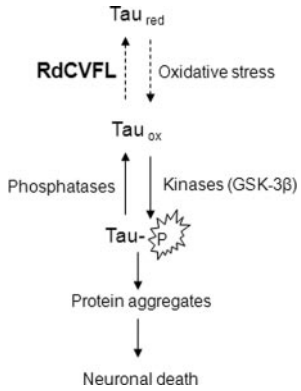

FIG. 10. **A model describing the role of RdCVFL-TAU interaction in the oxidative stress-induced retinal degeneration.** *red*, reduced; *ox*, oxidation.

redox status and therefore its phosphorylation/aggregation in the brain of aging humans. This novel signaling pathway may be implicated in neurodegenerative diseases such as AD in addition to retinal degeneration. In such cases, RdCVF proteins might be used broadly for treating patients suffering from these disorders by regulating oxidative stress (49).

Acknowledgments—We thank E. Clerin, W. Raffelsberger, D. Thiersé, S. Fouquet, and B. Kinzel.

* This work was supported by INSERM, Agence Nationale de Recherches, European Vision Institute-GENORET, European Union Grant MRTN-CT-2003-504003, and Retina France.

S The on-line version of this article (available at http://www.mcponline.org) contains supplemental material.

The nucleotide sequence(s) reported in this paper has been submitted to the GenBank™EBI Data Bank with accession number(s) EU380277 and EU380278.

** To whom correspondence should be addressed. Tel.: 33-1-53-46-25-48; Fax: 33-1-53-46-25-02; E-mail: Thierry.Leveillard@inserm.fr.

REFERENCES

1. Jones, D. P. (2006) Extracellular redox state: refining the definition of oxidative stress in aging. *Rejuvenation Res.* **9,** 169–181
2. Reynolds, A., Laurie, C., Mosley, R. L., and Gendelman, H. E. (2007) Oxidative stress and the pathogenesis of neurodegenerative disorders. *Int. Rev. Neurobiol.* **82,** 297–325
3. Lundmark, P. O., Pandi-Perumal, S. R., Srinivasan, V., Cardinali, D. P., and Rosenstein, R. E. (2007) Melatonin in the eye: implications for glaucoma. *Exp. Eye Res.* **84,** 1021–1030
4. Beatty, S., Koh, H., Phil, M., Henson, D., and Boulton, M. (2000) The role of oxidative stress in the pathogenesis of age-related macular degeneration. *Surv. Ophthalmol.* **45,** 115–134
5. Cingolani, C., Rogers, B., Lu, L., Kachi, S., Shen, J., and Campochiaro, P. A. (2006) Retinal degeneration from oxidative damage. *Free Radic. Biol. Med.* **40,** 660–669
6. Yu, D. Y., Cringle, S., Valter, K., Walsh, N., Lee, D., and Stone, J. (2004) Photoreceptor death, trophic factor expression, retinal oxygen status, and photoreceptor function in the P23H rat. *Investig. Ophthalmol. Vis. Sci.* **45,** 2013–2019
7. Komeima, K., Rogers, B. S., Lu, L., and Campochiaro, P. A. (2006) Antioxidants reduce cone cell death in a model of retinitis pigmentosa. *Proc. Natl. Acad. Sci. U. S. A.* **103,** 11300–11305
8. Yoshida, T., Oka, S., Masutani, H., Nakamura, H., and Yodoi, J. (2003) The role of thioredoxin in the aging process: involvement of oxidative stress. *Antioxid. Redox Signal.* **5,** 563–570
9. Tanito, M., Masutani, H., Nakamura, H., Oka, S., Ohira, A., and Yodoi, J. (2002) Attenuation of retinal photooxidative damage in thioredoxin transgenic mice. *Neurosci. Lett.* **326,** 142–146
10. Akterin, S., Cowburn, R. F., Miranda-Vizuete, A., Jimenez, A., Bogdanovic, N., Winblad, B., and Cedazo-Minguez, A. (2006) Involvement of glutaredoxin-1 and thioredoxin-1 in β-amyloid toxicity and Alzheimer's disease. *Cell Death Differ.* **13,** 1454–1465
11. Lovell, M. A., Xie, C., Gabbita, S. P., and Markesbery, W. R. (2000) Decreased thioredoxin and increased thioredoxin reductase levels in Alzheimer's disease brain. *Free Radic. Biol. Med.* **28,** 418–427
12. Saitoh, M., Nishitoh, H., Fujii, M., Takeda, K., Tobiume, K., Sawada, Y., Kawabata, M., Miyazono, K., and Ichijo, H. (1998) Mammalian thioredoxin is a direct inhibitor of apoptosis signal-regulating kinase (ASK) 1. *EMBO J.* **17,** 2596–2606
13. Lillig, C. H., and Holmgren, A. (2007) Thioredoxin and related molecules—from biology to health and disease. *Antioxid. Redox Signal.* **9,** 25–47
14. Leveillard, T., Mohand-Said, S., Lorentz, O., Hicks, D., Fintz, A. C., Clerin, E., Simonutti, M., Forster, V., Cavusoglu, N., Chalmel, F., Dolle, P., Poch, O., Lambrou, G., and Sahel, J. A. (2004) Identification and characterization of rod-derived cone viability factor. *Nat. Genet.* **36,** 755–759
15. Cronin, T., Leveillard, T., and Sahel, J. A. (2007) Retinal degenerations: from cell signaling to cell therapy; pre-clinical and clinical issues. *Curr. Gene Ther.* **7,** 121–129
16. Sahel, J. A. (2005) Saving cone cells in hereditary rod diseases: a possible role for rod-derived cone viability factor (RdCVF) therapy. *Retina* **25,** S38-S39
17. Arner, E. S., and Holmgren, A. (2000) Physiological functions of thioredoxin and thioredoxin reductase. *Eur. J. Biochem.* **267,** 6102–6109
18. Wang, X. W., Liou, Y. C., Ho, B., and Ding, J. L. (2007) An evolutionarily conserved 16-kDa thioredoxin-related protein is an antioxidant which regulates the NF-κB signaling pathway. *Free Radic. Biol. Med.* **42,** 247–259
19. Wang, X. W., Tan, B. Z., Sun, M., Ho, B., and Ding, J. L. (2008) Thioredoxin-like 6 protects retinal cell line from photooxidative damage by upregulating NF-κB activity. *Free Radic. Biol. Med.* **45,** 336–344
20. Pekkari, K., Avila-Carino, J., Gurunath, R., Bengtsson, A., Scheynius, A., and Holmgren, A. (2003) Truncated thioredoxin (Trx80) exerts unique mitogenic cytokine effects via a mechanism independent of thiol oxidoreductase activity. *FEBS Lett.* **539,** 143–148
21. Drubin, D. G., and Kirschner, M. W. (1986) Tau protein function in living cells. *J. Cell Biol.* **103,** 2739–2746
22. Grundke-Iqbal, I., Iqbal, K., Tung, Y. C., Quinlan, M., Wisniewski, H. M., and Binder, L. I. (1986) Abnormal phosphorylation of the microtubule-associated protein τ (tau) in Alzheimer cytoskeletal pathology. *Proc. Natl. Acad. Sci. U. S. A.* **83,** 4913–4917
23. Buee, L., Bussiere, T., Buee-Scherrer, V., Delacourte, A., and Hof, P. R. (2000) Tau protein isoforms, phosphorylation and role in neurodegenerative disorders. *Brain Res. Brain Res. Rev.* **33,** 95–130
24. Brandt, R., Hundelt, M., and Shahani, N. (2005) Tau alteration and neuronal degeneration in tauopathies: mechanisms and models. *Biochim. Biophys. Acta* **1739,** 331–354
25. Fintz, A. C., Audo, I., Hicks, D., Mohand-Said, S., Leveillard, T., and Sahel, J. (2003) Partial characterization of retina-derived cone neuroprotection in two culture models of photoreceptor degeneration. *Investig. Ophthalmol. Vis. Sci.* **44,** 818–825
26. Elias, J. E., and Gygi, S. P. (2007) Target-decoy search strategy for increased confidence in large-scale protein identifications by mass spectrometry. *Nat. Methods* **4,** 207–214
27. Peng, J., Elias, J. E., Thoreen, C. C., Licklider, L. J., and Gygi, S. P. (2003) Evaluation of multidimensional chromatography coupled with tandem mass spectrometry (LC/LC-MS/MS) for large-scale protein analysis: the yeast proteome. *J. Proteome Res.* **2,** 43–50
28. von Mering, C., Jensen, L. J., Kuhn, M., Chaffron, S., Doerks, T., Kruger, B., Snel, B., and Bork, P. (2007) STRING 7—recent developments in the integration and prediction of protein interactions. *Nucleic Acids Res.* **35,** D358–D362
29. Shannon, P., Markiel, A., Ozier, O., Baliga, N. S., Wang, J. T., Ramage, D., Amin, N., Schwikowski, B., and Ideker, T. (2003) Cytoscape: a software environment for integrated models of biomolecular interaction networks. *Genome Res.* **13,** 2498–2504
30. Sherman, B. T., Huang, D. W., Tan, Q., Guo, Y., Bour, S., Liu, D., Stephens, R., Baseler, M. W., Lane, H. C., and Lempicki, R. A. (2007) DAVID Knowledgebase: a gene-centered database integrating heterogeneous gene annotation resources to facilitate high-throughput gene functional analysis. *BMC Bioinformatics* **8,** 426
31. Chalmel, F., Leveillard, T., Jaillard, C., Lardenois, A., Berdugo, N., Morel, E., Koehl, P., Lambrou, G., Holmgren, A., Sahel, J. A., and Poch, O. (2007) Rod-derived Cone Viability Factor-2 is a novel bifunctional-thioredoxin-like protein with therapeutic potential. *BMC Mol. Biol.* **8,** 74
32. Tewari, M., Yu, M., Ross, B., Dean, C., Giordano, A., and Rubin, R. (1997) AAC-11, a novel cDNA that inhibits apoptosis after growth factor withdrawal. *Cancer Res.* **57,** 4063–4069
33. Solomon, S., Xu, Y., Wang, B., David, M. D., Schubert, P., Kennedy, D., and Schrader, J. W. (2007) Distinct structural features of caprin-1 mediate its interaction with G3BP-1 and its induction of phosphorylation of eukaryotic translation initiation factor 2α, entry to cytoplasmic stress granules, and selective interaction with a subset of mRNAs. *Mol. Cell. Biol.* **27,** 2324–2342
34. Goedert, M., Spillantini, M. G., Jakes, R., Rutherford, D., and Crowther, R. A. (1989) Multiple isoforms of human microtubule-associated protein tau: sequences and localization in neurofibrillary tangles of Alzheimer's disease. *Neuron* **3,** 519–526
35. Melov, S., Adlard, P. A., Morten, K., Johnson, F., Golden, T. R., Hinerfeld,

D., Schilling, B., Mavros, C., Masters, C. L., Volitakis, I., Li, Q. X., Laughton, K., Hubbard, A., Cherny, R. A., Gibson, B., and Bush, A. I. (2007) Mitochondrial oxidative stress causes hyperphosphorylation of tau. *PLoS ONE* **2,** e536

36. Ohsawa, I., Nishimaki, K., Murakami, Y., Suzuki, Y., Ishikawa, M., and Ohta, S. (2008) Age-dependent neurodegeneration accompanying memory loss in transgenic mice defective in mitochondrial aldehyde dehydrogenase 2 activity. *J. Neurosci.* **28,** 6239–6249
37. Lovestone, S., Reynolds, C. H., Latimer, D., Davis, D. R., Anderton, B. H., Gallo, J. M., Hanger, D., Mulot, S., Marquardt, B., Stabel, S., Woodgett, J. R., and Miller, C. C. J. (1994) Alzheimer's disease-like phosphorylation of the microtubule-associated protein tau by glycogen synthase kinase-3 in transfected mammalian cells. *Curr. Biol.* **4,** 1077–1086
38. Landino, L. M., Skreslet, T. E., and Alston, J. A. (2004) Cysteine oxidation of tau and microtubule-associated protein-2 by peroxynitrite: modulation of microtubule assembly kinetics by the thioredoxin reductase system. *J. Biol. Chem.* **279,** 35101–35105
39. Grundke-Iqbal, I., Iqbal, K., Quinlan, M., Tung, Y. C., Zaidi, M. S., and Wisniewski, H. M. (1986) Microtubule-associated protein tau. A component of Alzheimer paired helical filaments. *J. Biol. Chem.* **261,** 6084–6089
40. Schweers, O., Mandelkow, E. M., Biernat, J., and Mandelkow, E. (1995) Oxidation of cysteine-322 in the repeat domain of microtubule-associated protein tau controls the in vitro assembly of paired helical filaments. *Proc. Natl. Acad. Sci. U. S. A.* **92,** 8463–8467
41. Zhang, Y. Z., Gould, K. L., Dunbrack, R. J., Cheng, H., Roder, H., and Golemis, E. A. (1999) The evolutionarily conserved Dim1 protein defines a novel branch of the thioredoxin fold superfamily. *Physiol. Genomics* **1,** 109–118
42. Schmidt-Kastner, R., Yamamoto, H., Hamasaki, D., Yamamoto, H., Parel, J. M., Schmitz, C., Dorey, C. K., Blanks, J. C., and Preising, M. N. (2008) Hypoxia-regulated components of the U4/U6.U5 tri-small nuclear ribonucleoprotein complex: possible role in autosomal dominant retinitis pigmentosa. *Mol. Vis.* **14,** 125–135
43. Takahashi, N., Kariya, S., Hirano, M., and Ueno, S. (2003) Two novel spliced presenilin 2 transcripts in human lymphocyte with oxidant stress and brain. *Mol. Cell. Biochem.* **252,** 279–283
44. Nunomura, A., Perry, G., Aliev, G., Hirai, K., Takeda, A., Balraj, E. K., Jones, P. K., Ghanbari, H., Wataya, T., Shimohama, S., Chiba, S., Atwood, C. S., Petersen, R. B., and Smith, M. A. (2001) Oxidative damage is the earliest event in Alzheimer disease. *J. Neuropathol. Exp. Neurol.* **60,** 759–767
45. Fulga, T. A., Elson-Schwab, I., Khurana, V., Steinhilb, M. L., Spires, T. L., Hyman, B. T., and Feany, M. B. (2007) Abnormal bundling and accumulation of F-actin mediates tau-induced neuronal degeneration in vivo. *Nat. Cell Biol.* **9,** 139–148
46. Gomez-Ramos, A., Diaz-Nido, J., Smith, M. A., Perry, G., and Avila, J. (2003) Effect of the lipid peroxidation product acrolein on tau phosphorylation in neural cells. *J. Neurosci. Res.* **71,** 863–870
47. Mattson, M. P., Fu, W., Waeg, G., and Uchida, K. (1997) 4-Hydroxynonenal, a product of lipid peroxidation, inhibits dephosphorylation of the microtubule-associated protein tau. *Neuroreport* **8,** 2275–2281
48. Gupta, N., Fong, J., Ang, L. C., and Yucel, Y. H. (2008) Retinal tau pathology in human glaucomas. *Can. J. Ophthalmol.* **43,** 53–60
49. Yang, Y., Mohand-Said, S., Danan, A., Simonutti, M., Fontaine, V., Clerin, E., Picaud, P., Léveillard, T., and Sahel, J. A. (2009) Functional cone rescue by RdCVF protein in a dominant model of retinitis pigmentosa. *Mol. Ther.*, in press